JOURNAL OF THE AMERICAN CHEMICAL SOCIETY

Subscriber access provided by READING UNIV

Article

An Organometallic Cu20 Nanocluster: Synthesis, Characterization, Immobilization on Silica, and “Click” Chemistry

Andrew W. Cook, Zachary R. Jones, Guang Wu, Susannah L Scott, and Trevor W. Hayton

J. Am. Chem. Soc., **Just Accepted Manuscript** • DOI: 10.1021/jacs.7b10960 • Publication Date (Web): 06 Dec 2017

Downloaded from http://pubs.acs.org on December 6, 2017

Just Accepted

“Just Accepted” manuscripts have been peer-reviewed and accepted for publication. They are posted online prior to technical editing, formatting for publication and author proofing. The American Chemical Society provides “Just Accepted” as a free service to the research community to expedite the dissemination of scientific material as soon as possible after acceptance. “Just Accepted” manuscripts appear in full in PDF format accompanied by an HTML abstract. “Just Accepted” manuscripts have been fully peer reviewed, but should not be considered the official version of record. They are accessible to all readers and citable by the Digital Object Identifier (DOI®). “Just Accepted” is an optional service offered to authors. Therefore, the “Just Accepted” Web site may not include all articles that will be published in the journal. After a manuscript is technically edited and formatted, it will be removed from the “Just Accepted” Web site and published as an ASAP article. Note that technical editing may introduce minor changes to the manuscript text and/or graphics which could affect content, and all legal disclaimers and ethical guidelines that apply to the journal pertain. ACS cannot be held responsible for errors or consequences arising from the use of information contained in these “Just Accepted” manuscripts.

ACS Publications

Journal of the American Chemical Society is published by the American Chemical Society. 1155 Sixteenth Street N.W., Washington, DC 20036

Published by American Chemical Society. Copyright © American Chemical Society. However, no copyright claim is made to original U.S. Government works, or works produced by employees of any Commonwealth realm Crown government in the course of their duties.

An Organometallic Cu_{20} Nanocluster: Synthesis, Characterization, Immobilization on Silica, and “Click” Chemistry

Andrew W. Cook[†], Zachary R. Jones[‡], Guang Wu[†], Susannah L. Scott[‡]*, and Trevor W. Hayton[†]*

[†]Department of Chemistry and Biochemistry, University of California, Santa Barbara, California 93106, United States
[‡]Department of Chemical Engineering, University of California, Santa Barbara, California 93106, United States

Supporting Information Placeholder

ABSTRACT: The development of atomically-precise nanoclusters (APNCs) protected by organometallic ligands, such as acetylides and hydrides, is an emerging area of nanoscience. In principle, these organometallic APNCs should not require harsh pre-treatment for activation towards catalysis, such as calcination, which can lead to sintering. Herein, we report the synthesis of the mixed-valent organometallic copper APNC, $[Cu_{20}(CCPh)_{12}(OAc)_6)]$ (**1**), via reduction of Cu(OAc) with Ph_2SiH_2 in the presence of phenylacetylene. This cluster is a rare example of a two-electron copper superatom, and the first to feature a tetrahedral $[Cu_4]^{2+}$ core, which is a unique “kernel” for a Cu-only superatom. Complex **1** can be readily immobilized on dry, partially-dehydroxylated silica, a process that cleanly results in release of 1 equiv of phenylacetylene per Cu_{20} cluster. Cu K-edge EXAFS confirms that the immobilized cluster **2** is structurally similar to **1**. In addition, both **1** and **2** are effective catalysts for [3+2] cycloaddition reactions between alkynes and azides (i.e., “Click” reactions) at room temperature. Significantly, neither cluster requires any pre-treatment for activation toward catalysis. Moreover, EXAFS analysis of **2** after catalysis demonstrates that the cluster undergoes no major structural or nuclearity changes during the reaction, consistent with our observation that supported cluster **2** is more stable than unsupported cluster **1** under “Click” reaction conditions.

INTRODUCTION

Atomically-precise nanoclusters (APNCs) have been the subject of intense interest over the past decade for their use in a variety of emerging technological applications, including catalysis.[1-7] Significantly, their perfectly mono-disperse and atomically-precise nature permits their complete structural characterization, facilitating the development of detailed structure/activity relationships (SARs).[8-11] Yet, while the study of APNCs could uncover new insights in catalysis, many APNCs are actually not well-suited for this purpose. For example, the vast majority of the known nanoclusters have been synthesized with a passivating shell of thiolate capping ligands.[12] While such ligands impart significant thermal and chemical stability to APNCs, and are often required to render the APNCs isolable, they block active sites, and must be partially removed before catalysis can occur.[13-15] At the same time, the strength of the metal-sulfur bond often makes it difficult to remove the thiolate ligands efficiently.[16-18] For example, Jin and coworkers reported that pre-treatment of $Au_{25}(SR)_{18}/CeO_2$ (R = C_2H_4Ph) with O_2 at 150 °C was required to activate the material for catalytic CO oxidation.[19] Similarly, pre-treatment of $Au_{25}(SR)_{18}/TiO_2$ at 300 °C was required to activate this material for the catalytic semi-hydrogenation of internal alkynes.[20] The need for harsh conditions is significant because they can cause irreversible changes in the structure and/or nuclearity of the APNCs, which dramatically diminishes our ability to extract robust SARs using APNC catalysts. Notably, in both of the examples described above, the catalyst structure during and/or after activation was not determined.

To address this challenge, several research groups are developing APNCs which are not passivated by thiolate ligands, and which, in principle, should not require harsh pre-treatment for activation.[21] These organometallic APNCs are most commonly stabilized with hydrides (i.e., H^-) as capping ligands,[22-27] and more recently, acetylides (i.e., $RC\equiv C^-$).[28-40] For example, we reported the syntheses of $[Cu_{25}H_{22}(PPh_3)_{12}]Cl$ and

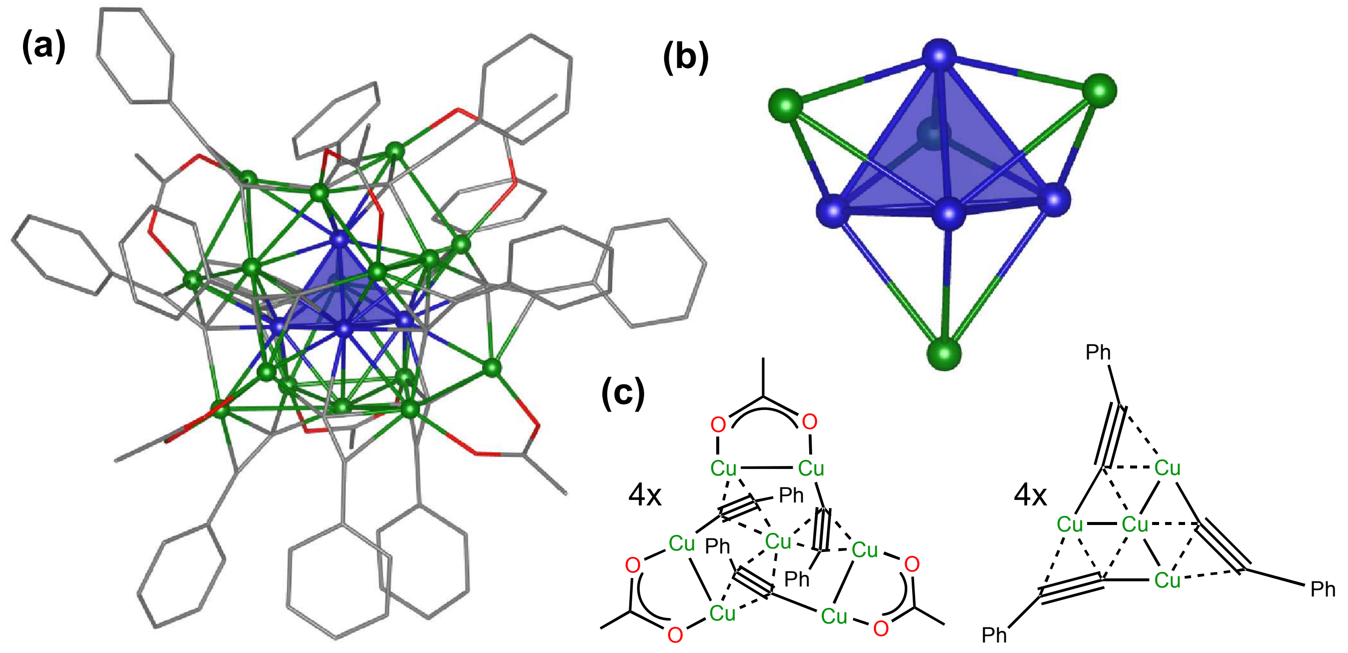

Figure 1. Ball and stick diagrams showing (a) complex **1**·C_4H_8O; (b) the tetrahedral Cu_4^{2+} core (blue), shown with face-capping copper atoms (green); and (c) illustrations of the ligand binding modes present in **1**·C_4H_8O. Hydrogen atoms, four THF solvate molecules and one coordinated THF molecule omitted for clarity. Color legend: Cu = blue, green; C = grey; O = red.

$[Cu_{29}Cl_4H_{22}(Ph_2phen)_{12}]Cl$ (Ph_2phen = 4,7-diphenyl-1,10-phenanthroline), both of which are ligated by a mix of hydride and neutral Lewis base ligands.[25, 27] Similarly, Liu and co-workers recently synthesized the copper acetylide nanocluster $[Cu_{13}\{S_2CN^nBu_2\}_6(CCR)_4][PF_6]$ (R = C(O)OMe, C_6H_4F), Zhang and co-workers generated the silver acetylide cluster $Ag_{74}(CCPh)_{44}$, and Wang and co-workers prepared the gold acetylide APNC $[Au_{19}(CCPh)_9(Hdppa)_3](SbF_6)_2$ (Hdppa = N,N-*bis*(diphenylphosphino)amine).[28, 33, 39]

Preliminary results suggest that organometallic APNCs are more reactive than their thiolate-capped cousins. For example, $[Au_{24}Ag_{20}(SPy)_4(CCPh)_{20}Cl_2]$ (SPy = 2-pyridylthiolate) was observed to release its phenylacetylide capping ligands at relatively low temperatures (~100 °C), although the cluster was not screened for any catalytic reactivity.[31] Also of note, Zheng and co-workers claimed that $[Au_{34}Ag_{28}(CCPh)_{34}]$ supported on XC-72 carbon was active for catalytic hydrolysis of triethylsilane without any pre-treatment.[41] One drawback of the above-mentioned study, however, is that the structure of the supported cluster was not interrogated. Therefore, it is still an open question whether organometallic APNCs maintain their structural integrity upon deposition onto a support. This concern is especially relevant for organometallic APNCs, given their higher thermal, oxygen, and water sensitivity, relative to thiolate-capped APNCs.[12, 41]

Herein, we report the synthesis and characterization of an unprecedented organometallic copper-based APNC, $[Cu_{20}(CCPh)_{12}(OAc)_6]$, and explore its ability to catalyze Huisgen [3+2] cycloadditions. Significantly, we find that the silica-immobilized cluster is a highly effective catalyst for this transformation. More importantly, the supported cluster is more stable under the "Click" reaction conditions than is the unsupported cluster. We have also confirmed that the supported cluster, both pre- and post-catalysis, has not undergone any major structural and/or nuclearity changes relative to the unsupported cluster. This study demonstrates for the first time that organometallic APNCs can maintain their structural integrity during catalysis, permitting the development of SARs for these unique nanomaterials.

RESULTS AND DISCUSSION

Synthesis of a Cu_{20} nanocluster. Addition of 0.6 equiv of phenylacetylene (HCCPh) to a slurry of Cu(OAc) (1 equiv) in THF results in a rapid color change from pale green to bright yellow, characteristic of the known Cu(I) coordination polymer, $[Cu(CCPh)]_n$,[42] concomitant with the generation of HOAc.[42-43] Addition of 0.36 equiv of diphenylsilane (Ph_2SiH_2) to this slurry results in a gradual color change to dark red-brown, accompanied by the appearance of a dark brown powder. Work-up of the solution after stirring at room temperature for 15 h resulted in the isolation of the mixed-valent copper acetylide nanocluster, $[Cu_{20}(CCPh)_{12}(OAc)_6]$ (**1**), as a red-orange, crystalline solid in 49% yield (Scheme 1a). Copper metal is also formed during the reaction, and was isolated in 42% yield (based on Cu(OAc)) by filtration of the reaction mixture through a 0.2 µm PTFE filter. The presence of the by-product $Ph_2Si(OAc)_2$ was confirmed by ^1H NMR spectroscopy of the supernatant (see Figure S3). For comparison, the only other Cu acetylide nanocluster, $[Cu_{13}\{S_2CN^nBu_2\}_6(CCR)_4][PF_6]$ (R = C(O)OMe, C_6H_4F), was formed during semihydrogenation of an alkyne by the Cu(I) hydride nanocluster $[Cu_{28}H_{15}\{S_2CN^nBu_2\}_{12}][PF_6]$.[33]

Scheme 1. Syntheses of complex 1

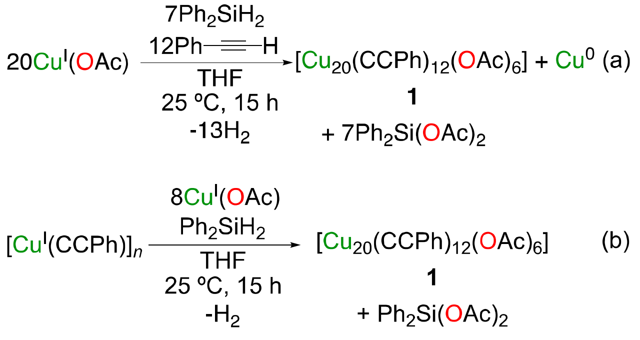

Complex **1** crystallizes as the THF adduct, **1**·C_4H_8O, as red blocks in the triclinic space group $P\bar{1}$ (Figure 1). Four additional THF molecules are incorporated into the crystal lattice as solvates. In the solid state, **1**·C_4H_8O contains a tetrahedral $[Cu_4]^{2+}$ core (Figure 1b). Encapsulating the tetrahedral core is a $[Cu_{16}(CCPh)_{12}(OAc)_6]^{2-}$ shell. The Cu-Cu distances within the cluster span a large range (2.463(3) – 2.934(3) Å), similar to other structurally characterized copper nanoclusters.[25, 27, 33, 44-45] The twelve acetylide ligands incorporated into the $[Cu_{16}(CCPh)_{12}(OAc)_6]^{2-}$ shell are arranged in four [*cyclo*-Cu(CCPh)]$_3$ units, which are situated at the vertices of a tetrahedron (Figure 1c). One acetylide ligand features a μ_4:η^1,η^1,η^2,η^2 binding mode, four of the acetylide ligands feature a μ_3:η^1,η^1,η^2 binding mode, and seven feature a μ_4:η^1,η^1,η^1,η^2 binding mode. The six acetate ligands are bound in κ^2 fashion, are located on the edges of the tetrahedron, and feature an average Cu-O distance of 1.96(2) Å (Figure 1c). To the best of our knowledge, complex **1** is the first group 11 nanocluster to incorporate acetate co-ligands.[12] Additionally, a THF molecule is coordinated to Cu18, with a Cu–O bond distance of 2.47(1) Å. Consequently, complex **1**·C_4H_8O exhibits no symmetry in the solid state. However, NMR spectroscopic characterization in CD_2Cl_2 demonstrates that complex **1** exhibits idealized T_d symmetry in solution (*vide infra*), suggesting that this THF molecule is only weakly bound to the cluster. This observation also suggests that the acetylide ligands interconvert between the three observed binding modes.

Interestingly, because there are only 18 anionic ligands (12 acetylides and six acetates), two of the 20 Cu atoms in **1** must have a formal oxidation state of 0 to maintain charge balance. Accordingly, complex **1** can be viewed as a superatom with a magic number N* = 2 and an $[M_4]^{2+}$ core.[1, 25, 27, 33-34, 40, 46-48] This is a relatively uncommon magic number, and a rare core structure, for group 11 superatoms.[39, 41, 44-45, 49-51] Almost all structurally characterized superatoms, such as the related copper acetylide superatom, $[Cu_{13}\{S_2CN^nBu_2\}_6(CCR)_4][PF_6]$,[33] contain metal-centered icosahedral, cuboctahedral, or anticuboctahedral cores.[12, 25, 27, 40, 45-51] In complex **1**, no such central metal atom is present, therefore the two "extra" electrons most likely occupy the a_1 symmetric bonding molecular orbital formed from the linear combination of the four Cu 4s orbitals within the tetrahedral $[Cu_4]^{2+}$ core. The three t_2 symmetric orbitals remain unoccupied.[52] The unique core structure and incorporation of acetate ligands in **1** expands the structural diversity of copper superatoms, and raises the possibility that many more copper superatoms, with a wide variety of ligand types, should be isolable.

Both the ^{1}H and ^{13}C{^{1}H} NMR spectra of **1** in CD_2Cl_2 are consistent with a T_d-symmetric structure in solution. For example, the ^{1}H NMR spectrum of **1** features a singlet at 2.01 ppm, integrating for 18 protons, assigned to the six magnetically equivalent acetate ligands. In addition, resonances at 7.41, 7.15, and 6.95 ppm, integrating for 24, 12, and 24 protons, respectively, are assigned to the *o*-Ph, *p*-Ph, and *m*-Ph environments of 12 magnetically equivalent phenylacetylide ligands. The ^{13}C{^{1}H} NMR spectrum of **1** features a resonance at 23.31 ppm, which is assigned to the methyl groups of the acetate co-ligands, while a resonance at 135.31 ppm is assigned to the Cu-bound acetylide carbons. Electrospray ionization mass spectroscopy (ESI-MS) of isolated complex **1** in THF, acquired in positive ion mode, is consistent with our proposed formulation (Figure S17). The major features, at *m/z* 2778.1309 and 2902.0662, correspond to $[M - OAc]^+$ (calcd *m/z* 2778.1221) and $[M + Cu]^+$ (calcd *m/z* 2902.0608) ions, respectively.

We also briefly examined the chemical properties of **1**. It is soluble in benzene, toluene, THF, and CH_2Cl_2, but insoluble in MeCN, Et_2O, and nonpolar solvents. It is stable in CD_2Cl_2 for at least 48 h, and stable to air and water (as a CD_2Cl_2 solution) for up to 24 h. As a solid, complex **1** shows no signs of decomposition after 2 months of exposure to air and water on the bench top. We also explored the electrochemical properties of complex **1** in CH_2Cl_2 at 25 °C. The cyclic voltammogram of **1** features two irreversible oxidation events at E = 0.20 and 0.55 V (vs. Fc/Fc$^+$) (Figure S24). These features remain irreversible, even at scan rates of up to 2000 mV s^{-1}. We hypothesize that electrons are being removed from the a_1 symmetric bonding orbital, disrupting the Cu-Cu bonding network, and resulting in rapid decomposition of the cluster.[52] For comparison, the related Cu_{13} cluster, $[Cu_{13}\{S_2CN^nBu_2\}_6(CCR)_4][PF_6]$ (R = C(O)OMe), exhibits two comparable quasi-reversible oxidation features (-0.05 and 0.34 V, vs. Fc/Fc$^+$), which the authors also ascribe to removal of Cu-Cu bonding electrons.[33] The cyclic voltammogram of **1** also features an irreversible reduction event at –1.02 V, which only appears after sampling the two irreversible oxidations. These observations are suggestive of an *ECE*-type process, but the identity of the species responsible for reduction feature is not known at this time.

Mechanistic Considerations. The first step in the formation of complex **1** appears to be the generation of the well-known yellow Cu(I) coordination polymer [Cu(CCPh)]$_n$, along with HOAc.[42-43] Ph_2SiH_2 then reacts with HOAc to make H_2 and $Ph_2Si(OAc)_2$. In parallel, we surmise that Ph_2SiH_2 also reacts with unconsumed Cu(OAc) to give Cu(0), which is captured by [Cu(CCPh)]$_n$ to generate the final nanocluster product. This mechanism is consistent with the formation of the yellow solid we observe in the reaction mixture at short reaction times. It is also consistent with the observation of bulk Cu metal in the reaction mixture, which is likely formed when some of the Cu(0) source is not captured by [Cu(CCPh)]$_n$ during the reaction, and eventually precipitates as bulk copper metal.

To test this hypothesis, we attempted the synthesis of **1** using a mixture of Cu(OAc) (8 equiv) and independently-synthesized [Cu(CCPh)]$_n$ (12 equiv) as Cu sources (Scheme 1b). Reaction of this combination with Ph_2SiH_2 (1 equiv) in THF for 30 h resulted in the formation of a red-orange THF solution and a green-brown solid. Work-up of the THF-soluble fraction resulted in the isolation of **1** in 26% yield. While its yield is low, the formation of **1** under these conditions is consistent with our proposed mechanism. Additionally, the reaction of Ph_2SiH_2 with 95% HOAc in CD_3CN, in the presence of 10 mol% of Cu(OAc), resulted in rapid formation of H_2,

$Ph_2SiH(OAc)$ and $Ph_2Si(OAc)_2$, according to ^{1}H NMR spectroscopy (Figure S5), confirming our hypothesis regarding the mechanism of formation of $Ph_2Si(OAc)_2$. Interestingly, no reaction between Ph_2SiH_2 and HOAc was observed in the absence of Cu(OAc).

We also attempted the synthesis of **1** in the presence of excess Ph_2SiH_2 (10 equiv total). Under these conditions, we observed almost exclusive formation of Cu^0. Thus, it appears that when **1** is formed in the presence of unreacted silane, the cluster rapidly decomposes. Consistent with this observation, reaction of **1** with 3 equiv of Ph_2SiH_2 in CD_2Cl_2 resulted in decomposition of **1** and formation of Cu metal as the only identifiable Cu-containing material (Figure S4).

Several groups,[12] including ours,[25] have demonstrated that the metal:ligand ratio employed during nanocluster syntheses can affect the final cluster size. In the system described here, however, increasing the Cu(OAc):alkyne ratio to 20:6 (from 20:12 used in Scheme 1a), in an attempt to isolate a larger nanocluster, resulted only in formation of copious amounts of Cu metal (and no tractable Cu acetylide clusters). Decreasing the Cu(OAc):alkyne ratio to 20:20 still resulted in the formation of complex **1**, but in a lower isolated yield.

*Grafting of **1** onto Silica.* We also explored the reaction of **1** with dehydrated and partially-dehydroxylated silica (Sylopol 952, pretreated in vacuum at 200 °C). Reaction of a red C_6D_6 solution of **1** with 36.0 mg silica (to give a solid containing ca. 3 wt% Cu) results in gradual transfer of **1** from solution to the silica (1 h total reaction time), to provide an orange solid and a colorless solution. A solution-state ^{1}H NMR spectrum of the reaction supernatant after 1 h revealed a complete absence of peaks assignable to **1**, as well as formation of 1 equiv of PhCCH (Scheme 2 and Figure S6). We see no evidence for formation of HOAc in solution, consistent with the relative basicities of $[OAc]^-$ and $[PhCC]^-$. To explain these observations, we suggest that reaction of **1** with a surface hydroxyl group (≡SiOH) results in protonation of one acetylide ligand of **1** and formation of immobilized cluster **2** via a new Cu-O-Si bond.

Scheme 2. Reaction of 1 with Silica

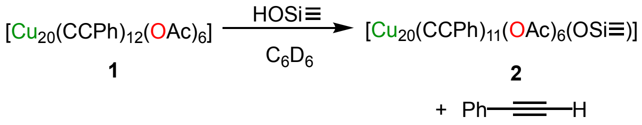

*"Click" Chemistry with **1** and **2**.* Copper-catalyzed [3+2] Huisgen cycloadditions of terminal alkynes and organic azides (CuAAC) have been the cornerstone of "Click" chemistry since the seminal reports of Meldal and Sharpless in 2002.[53-54] Recently, Straub and co-workers reported that a small Cu(I) acetylide cluster was a competent catalyst for the "Click" reaction.[55] Intriguingly, that cluster features acetylide ligands with μ_4:η^1,η^1,η^1,η^2 and μ_3:η^1,η^1,η^2 binding modes, which are nearly identical to those observed in complex **1**.[55] Thus, we hypothesized that **1** would also be a competent catalyst for the same transformation. Accordingly, we examined the ability of **1** to catalyze the [3+2] cycloaddition of several alkynes (HCCR, R = Ph, CO_2Et, and ^{t}Bu) with benzyl azide. Addition of **1** (0.5 mol% Cu_{20} cluster) to a CD_2Cl_2 solution of benzyl azide (1.1 equiv) and HCCPh (1 equiv), at room temperature, generated 1-benzyl-4-phenyl-1*H*-1,2,3-triazole (**3**) in good yield (entry 1, Table 1). Complex **1** is also effective at a much lower catalyst loading (0.05 mol% Cu_{20} cluster, entry 2, Table 1). Comparable yields of triazoles ethyl-1-benzyl-1H-1,2,3-triazole-4-carboxylate (**4**) and 1-benzyl-4-tert-butyl-1H-1,2,3-triazole (**5**) were observed upon substitution of HCCPh with either $HCC(CO_2Et)$ or HCC^{t}Bu, respectively (entries 3 and 4, Table 1). Notably, however, in these two cases we also observe the formation of **3** in the reaction mixture (see Figures S14 and S15), indicating that the phenylacetylide ligands present in **1** play a role in the catalytic cycle and can be incorporated into the product. To rationalize this observation, we propose that the first step of the catalytic cycle involves reaction of benzyl azide with a bound phenylacetylide ligand, resulting in formation of a copper-bound triazolate fragment.[56] This fragment undergoes subsequent protonolysis by incoming alkyne to generate **3** and a new copper-bound acetylide ligand.

Interestingly, as the homogeneous catalytic reaction proceeds, the red-orange color of **1** slowly disappears and a bright yellow solid resembling $[Cu(CCPh)]_n$ begins to precipitate from the reaction mixture.[42] This phenomenon was observed for all three alkyne substrates. Additionally, the ^{1}H NMR signals attributed to complex **1** lose > 95% of their intensity (relative to the internal standard) over the course of the reaction. These data suggest that **1** has somewhat limited stability under the reaction conditions, and likely dissociates into smaller clusters and/or discrete Cu^+ ions, either of which may also be catalytically active.[57] Accordingly, we cannot definitively conclude that complex **1** is the active catalyst in this system, and it may simply function as a pre-catalyst. Similar behavior has been observed in other Cu nanoparticle systems.[58-59]

We also examined the ability of heterogeneous **2** to catalyze the [3+2] cycloaddition of phenylacetylene and benzyl azide, under conditions identical to those employed in the homogeneous reaction. Thus, addition of **2** (0.5 mol% Cu_{20} cluster) to a CD_2Cl_2 solution of benzyl azide (1.1 equiv) and HCCPh (1 equiv) generated **3** in comparable yields to those observed using intact **1** (entry 5, Table 1). The recycled silica-supported catalyst also generated **3** in comparable yield (entry 6, Table 1). Notably, we see no evidence for leaching of complex **1** from the SiO_2 support into CD_2Cl_2 over 7 h by ^{1}H NMR spectroscopy, either in the absence or presence of the alkyne and azide substrates (Figures S16 and S9). Supported cluster **2** is also an effective catalyst for the [3+2] cycloaddition reaction at 40 °C (entry 7, Table 1). However, at these elevated temperatures, the catalyst undergoes a gradual color change from red-orange to pale yellow over the course of the reaction, suggesting that it may undergo a structural change upon heating.

It is well known that solvated Cu^+ ions can effectively catalyze the Click reaction.[43, 57] As a result, it has been a challenge to establish if Cu nanomaterials themselves are the actual catalysts or if leached Cu^+ ions are responsible for the observed reactivity.[60] To probe the stability of **2**, we separated the supported catalyst from the supernatant of a reaction between benzyl azide and HCCPh by filtration, then exposed the supernatant to fresh substrate (Figure S11). Under these conditions, we observed no conversion of alkyne and benzyl azide to the triazole after 7 h, suggesting that Cu^+ ions were not leached from the supported catalyst into solution over the course of the initial reaction. Overall, this result suggests that **2** is more stable than **1** under "Click" reaction conditions.

Table 1. [3+2] cycloadditions between benzyl azide and various terminal alkynes catalyzed by 1 and 2.[a]

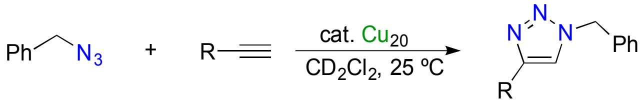

Entry	R	time (h)	loading (mol %)[b]	yield (%)[c]	TON
1	Ph	5	0.5	95	190
2	Ph	7	0.05	85	1700
3	CO_2Et	5	0.5	86	172
4	^{t}Bu	5	0.5	92	184
5	Ph	7	0.5[d]	95	190
6	Ph	7	0.5[e]	94	188
7[f]	Ph	2	0.5	>99	198

[a]For experimental details, see Supporting Information. [b]Catalyst loading defined as mol% Cu_{20} cluster. [c]Yield of triazole determined by integration of ^{1}H NMR spectra acquired with a 60 s pulse delay, using hexamethyldisiloxane as internal standard. [d]Catalyst immobilized on SiO_2 (see SI for experimental details). [e]Recovered catalyst, still immobilized on SiO_2 (see SI for experimental details). [f]Reaction performed at 40 °C.

For comparison, several groups have shown that supported copper nanomaterials can catalyze CuAAC chemistry.[58, 61-68] Broadly speaking, these materials exhibit activities and recyclabilities similar to those observed for **2**. However, many of these nanomaterials feature large polydispersities,[69-71] or suffer from ill-defined surface chemistries.[61, 63] As such, it is a challenge to reliably and predictably deposit these material on a support. Additionally, this polydispersity makes it a significant challenge to extract SARs in an effort to develop better catalyst systems.

*Characterization of **1** and **2** by X-ray Absorption Spectroscopy.* Previous studies[25, 27] on Cu-based APNCs revealed remarkable XAS sensitivity to both ligand sets and Cu nuclearity. Therefore, Cu K-edge XAFS was undertaken to compare structural features of complex **1** with its silica-supported analog, **2**, as well as the recovered post-catalysis material, $\mathbf{2_{post}}$. The absence of significant differences in the XANES profiles of **1** and **2** suggests that the nanocluster structure is preserved upon grafting onto SiO_2 (Figure S27). In the EXAFS, two prominent features appear at 1.6 and 2.3 Å in the FT magnitude of the EXAFS of **1** (Figure 2). The first peak represents light atoms directly coordinated to Cu, i.e., the donor atoms of the bidentate acetate and side-on bound acetylide ligands. The second peak represents the contributions of the Cu-Cu paths.

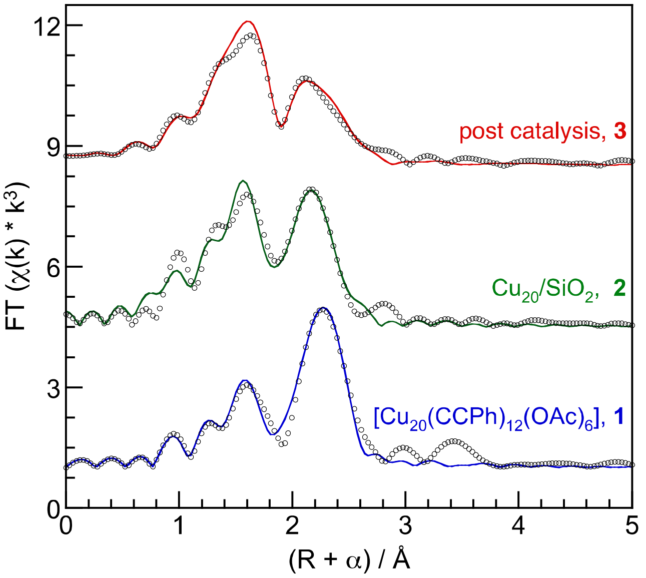

Figure 2. Comparison of Cu K-edge EXAFS (displayed as FT magnitude, points, with curvefits, lines) for $[Cu_{20}(CCPh)_{12}(OAc)_6]$ (1, blue), freshly-prepared Cu_{20}/SiO_2 (2, green), and post-catalysis Cu_{20}/SiO_2 (2_{post}, red).

The curvefit of the EXAFS of **1** (Figure S30) includes a Cu–O path and a Cu–C path, whose distances were fixed at the most commonly observed values in the X-ray crystal structure (1.951 and 2.061 Å, respectively, the latter being the distance corresponding to the Cu-C π-bonds). The fit returned *N*(Cu–O) and *N*(Cu–C) values of 0.6(3) and 1.2(4), respectively (Table 2). The number of Cu-O paths agrees with the average number of bidentate acetate ligands per Cu (0.3), while the value for the Cu–C path exceeds the average number of acetylide ligands per Cu (0.6), as expected due to the presence of both □- and π-interactions involving these ligands. The Cu-Cu paths, which range from 2.471 to 3.085 Å in the crystal structure, were represented in the curvefit by two paths whose distances were fixed at the most frequent Cu-Cu bond lengths. The resulting fit returned a combined *N*(Cu-Cu) of 2.3(5), similar to the crystallographically-determined value of 2.7.

The EXAFS of silica-supported **2** features two similar peaks, at 1.6 and 2.2 Å, with slightly different relative intensities compared to those observed for **1** (Figure 2). The distances for the Cu-O and Cu-C paths were again fixed using the most common values found in the molecular cluster **1**, while both coordination numbers were refined. Minor changes in the fitted values of *N*(Cu–O) and *N*(Cu–C), to 1.0(1) and 0.6(4), respectively, are consistent with a reaction of **1** with silica, which results in one acetylide ligand being replaced by a surface silyloxide (likely in a bridging configuration), among other possible interactions (see Figure S31 and Table 2). Although the intensity of the peak in the FT magnitude corresponding to the Cu-Cu paths decreased slightly upon deposition onto silica, curvefitting returned a similar total value for *N*(Cu–Cu), 2.3(3). We hypothesize that the Cu-Cu distribution becomes less uniform upon deposition, and the number of longer paths increases at the expense of the shorter paths. The resulting destructive interference results in an overall decrease in FT magnitude, without any cluster fragmentation. Thus, our EXAFS analysis suggests that immobilization of **1** results in little or no change to the cluster nuclearity, and only minor changes to the cluster structure.

Table 2. Curvefit parameters for the Cu K-edge EXAFS[a]

Material	Path	EXAFS curvefit		
		N	R(Å)	10^3 σ^2(Å^{-1})
1[b]	Cu-O	0.6(3)	1.951[c]	5(3)[d]
	Cu-C	1.2(4)	2.061[c]	5(3)[d]
	Cu-Cu1	2.1(5)	2.563[c]	6(2)[e]
	Cu-Cu2	0.2(1)	2.671[c]	6(2)[e]
2[f]	Cu-O	1.0(1)	1.951[c]	7(2)[d]
	Cu-C	0.6(4)	2.061[c]	7(2)[d]
	Cu-Cu1	1.7(2)	2.505(6)	7(2)[e]
	Cu-Cu2	0.6(2)	2.62(2)	7(2)[e]
$\mathbf{2}_{\mathbf{post}}$[g]	Cu-O	1.7(3)	1.951[c]	7(1)[d]
	Cu-C	0.7(3)	2.061[c]	7(1)[d]
	Cu-Cu1	1.2(3)	2.53(4)	6(1)[e]
	Cu-Cu2	0.5(3)	2.66(1)	6(1)[e]

[a] Uncertainties in the last significant figure are shown in parentheses. Values without uncertainties were fixed at values determined by X-ray crystallography. [b] Global fit parameters: $S_o^2 = 0.8(1)$; $\Delta E_o = 5(1)$ eV. [c] Fixed at values determined by single crystal X-ray diffraction (this work). [d] Constrained to have the same mean-squared displacement. [e] Constrained to have the same mean-squared displacement. [f] Global fit parameters: $S_o^2 = 0.8(2)$; $\Delta E_o = 8(2)$ eV. [g] Global fit parameters: $S_o^2 = 0.8(1)$; $\Delta E_o = 9(1)$ eV.

The supported cluster material was recovered after use as a catalyst for the cycloaddition of benzyl azide and HCCPh. The EXAFS of the recovered post-catalysis material, $\mathbf{2}_{\mathbf{post}}$, is again similar to that of the immobilized cluster **2** (Figure 2). The curvefit reveals an increase in *N*(Cu-O), to 1.7(3), while the value for *N*(Cu-C) remains essentially unchanged at 0.7(3) (Figure S32 and Table 2). The peak arising from the Cu-Cu paths broadened, while the total value of *N*(Cu-Cu) decreased to 1.7(5). Although these values are slightly different than those found for **2**, qualitative inspection of the spectrum for $\mathbf{2}_{\mathbf{post}}$ suggests that the supported cluster's ligand complement is largely preserved, i.e., there has been minimal rearrangement of the Cu-Cu skeleton. More importantly, these changes are not consistent with extensive cluster fragmentation or aggregation. The qualitative similarities in the EXAFS are also consistent with the XANES profiles of **2** and $\mathbf{2}_{\mathbf{post}}$, which show nearly indistinguishable, superimposable edges and absorbance maxima (Figure S27 and Table S3).

There are only a handful of prior reports describing the characterization of APNCs before and after deposition onto a solid support. For example, Spivey and co-workers demonstrated by EXAFS that deposition of a thiolate-capped Au_{38} cluster on TiO_2 resulted in aggregation.[72] In contrast, Wu and co-workers concluded that deposition of a Au_{22} nanocluster onto TiO_2 resulted in no agglomeration, on the basis of HAADF–STEM imaging.[73] While this cluster was competent for CO oxidation, the post-catalysis cluster was not characterized, so its nuclearity is unknown. Similarly, Scott and co-workers demonstrated that thiolate-protected Au_{25}(11-MUA)$_{18}$ (11-MUA = mercaptoundecanoic acid) maintained its structure after deposition onto SiO_2, but agglomerated upon calcination at 250 °C.[18] Thus, the nanocluster series **1**, **2**, and $\mathbf{2}_{\mathbf{post}}$ represents an exceptionally rare example of retention of cluster structure after deposition on a solid support, and after use in a catalytic reaction.

CONCLUSION

In summary, we have synthesized and characterized the novel organometallic nanocluster [Cu_{20}(CCPh)$_{12}$(OAc)$_6$] (**1**). Complex **1** is a rare example a 2-electron copper superatom, and the first copper superatom to feature a $[Cu_4]^{2+}$ core. Complex **1** can be readily immobilized on dry, partially-dehydroxylated silica, a process that results in release of 1 equiv of phenylacetylene per Cu_{20} cluster. According to qualitative and quantitative EXAFS analysis, the immobilized cluster **2** is structurally similar to **1**. In addition, both **1** and **2** are effective catalysts for [3+2] cycloaddition of alkynes and azide at room temperature. Intriguingly, supported cluster **2** appears to be substantially more stable than **1** under the reaction conditions. More importantly, however, neither **1** nor **2** require harsh pretreatment for activation, demonstrating the innate promise of organometallic APNCs for development of SARs in the field of supported catalysis.

ASSOCIATED CONTENT

Supporting Information

The Supporting Information is available free of charge on the ACS Publications website.

X-ray data for compound **1**·$5C_4H_8O$ (CIF)

Experimental procedures, crystallographic details, and spectral data (PDF)

AUTHOR INFORMATION

Corresponding Author

*hayton@chem.ucsb.edu
*sscott@engineering.ucsb.edu

Notes

The authors declare no competing financial interest.

ACKNOWLEDGMENT

T.W.H. and A.W.C. thank the National Science Foundation (CHE 1361654) for financial support. Z. J. and S. L. S. thank the U.S. Department of Energy, Office of Science, Office of Basic Energy Sciences, under the Catalysis Science Initiative (DE-FG-02-03ER15467), and the NSF PIRE program (OISE-0968399), for financial support. NMR spectra were collected on an instrument supported by an NIH Shared Instrumentation Grant (SIG, 1S10OD012077-01A1). ESI mass spectra were acquired at the MRL Shared Experimental Facilities, supported by the MRSEC Program of the NSF under Award No. DMR 1121053 and a member of the NSF-funded Materials Research Facilities Network. X-ray absorption spectra were acquired at the Stanford Synchrotron Radiation Lightsource, a Directorate of SLAC National Accelerator Laboratory and an Office of Science User Facility operated for the U.S. Department of Energy Office of Science by Stanford University. A. W. C. thanks the Mellichamp Academic Initiative in Sustainability at UCSB for a summer fellowship.

REFERENCES

1. Hakkinen, H., *Chem. Soc. Rev.* **2008**, *37*, 1847-1859.
2. Schmid, G., *Chem. Soc. Rev.* **2008**, *37*, 1909-1930.

3. Li, G.; Jin, R., *Acc. Chem. Res.* **2013**, *46*, 1749-1758.
4. Yamazoe, S.; Koyasu, K.; Tsukuda, T., *Acc. Chem. Res.* **2014**, *47*, 816-824.
5. Daniel, M.-C.; Astruc, D., *Chem. Rev.* **2004**, *104*, 293-346.
6. Parker, J. F.; Fields-Zinna, C. A.; Murray, R. W., *Acc. Chem. Res.* **2010**, *43*, 1289-1296.
7. Harkness, K. M.; Tang, Y.; Dass, A.; Pan, J.; Kothalawala, N.; Reddy, V. J.; Cliffel, D. E.; Demeler, B.; Stellacci, F.; Bakr, O. M.; McLean, J. A., *Nanoscale* **2012**, *4*, 4269-4274.
8. Yan, N.; Yuan, Y.; Dyson, P. J., *Dalton Trans.* **2013**, *42*, 13294-13304.
9. Zhu, Y.; Qian, H.; Drake, B. A.; Jin, R., *Angew. Chem. Int. Ed.* **2010**, *49*, 1295-1298.
10. Zhu, Y.; Qian, H.; Jin, R., *Chem. Eur. J.* **2010**, *16*, 11455-11462.
11. Zhu, Y.; Qian, H.; Jin, R., *J. Mater. Chem.* **2011**, *21*, 6793-6799.
12. Jin, R.; Zeng, C.; Zhou, M.; Chen, Y., *Chem. Rev.* **2016**, *116*, 10346-10413.
13. Das, S.; Goswami, A.; Hesari, M.; Al-Sharab, J. F.; Mikmeková, E.; Maran, F.; Asefa, T., *Small* **2014**, *10*, 1473-1478.
14. Elliott, E. W.; Glover, R. D.; Hutchison, J. E., *ACS Nano* **2015**, *9*, 3050-3059.
15. Wang, L.; Tang, Z.; Yan, W.; Yang, H.; Wang, Q.; Chen, S., *ACS Appl. Mater. Interfaces* **2016**, *8*, 20635-20641.
16. Ma, G.; Binder, A.; Chi, M.; Liu, C.; Jin, R.; Jiang, D.-e.; Fan, J.; Dai, S., *Chem. Commun.* **2012**, *48*, 11413-11415.
17. Fang, J.; Li, J.; Zhang, B.; Yuan, X.; Asakura, H.; Tanaka, T.; Teramura, K.; Xie, J.; Yan, N., *Nanoscale* **2015**, *7*, 6325-6333.
18. Sudheeshkumar, V.; Shivhare, A.; Scott, R. W. J., *Catal. Sci. Tech.* **2017**, *7*, 272-280.
19. Nie, X.; Qian, H.; Ge, Q.; Xu, H.; Jin, R., *ACS Nano* **2012**, *6*, 6014-6022.
20. Li, G.; Jin, R., *J. Am. Chem. Soc.* **2014**, *136*, 11347-11354.
21. Liu, P.; Qin, R.; Fu, G.; Zheng, N., *J. Am. Chem. Soc.* **2017**, *139*, 2122-2131.
22. Edwards, A. J.; Dhayal, R. S.; Liao, P.-K.; Liao, J.-H.; Chiang, M.-H.; Piltz, R. O.; Kahlal, S.; Saillard, J.-Y.; Liu, C. W., *Angew. Chem. Int. Ed.* **2014**, *53*, 7214-7218.
23. Dhayal, R. S.; Liao, J.-H.; Kahlal, S.; Wang, X.; Liu, Y.-C.; Chiang, M.-H.; van Zyl, W. E.; Saillard, J.-Y.; Liu, C. W., *Chem. Eur. J.* **2015**, *21*, 8369-8374.
24. Nguyen, T.-A. D.; Goldsmith, B. R.; Zaman, H. T.; Wu, G.; Peters, B.; Hayton, T. W., *Chem. Eur. J.* **2015**, *21*, 5341-5344.
25. Nguyen, T.-A. D.; Jones, Z. R.; Goldsmith, B. R.; Buratto, W. R.; Wu, G.; Scott, S. L.; Hayton, T. W., *J. Am. Chem. Soc.* **2015**, *137*, 13319-13324.
26. Dhayal, R. S.; van Zyl, W. E.; Liu, C. W., *Acc. Chem. Res.* **2016**, *49*, 86-95.
27. Nguyen, T.-A. D.; Jones, Z. R.; Leto, D. F.; Wu, G.; Scott, S. L.; Hayton, T. W., *Chem. Mater.* **2016**, *28*, 8385-8390.
28. Wan, X.-K.; Tang, Q.; Yuan, S.-F.; Jiang, D.-e.; Wang, Q.-M., *J. Am. Chem. Soc.* **2015**, *137*, 652-655.
29. Wan, X.-K.; Yuan, S.-F.; Tang, Q.; Jiang, D.-e.; Wang, Q.-M., *Angew. Chem. Int. Ed.* **2015**, *54*, 5977-5980.
30. Wan, X.-K.; Xu, W. W.; Yuan, S.-F.; Gao, Y.; Zeng, X.-C.; Wang, Q.-M., *Angew. Chem. Int. Ed.* **2015**, *54*, 9683-9686.
31. Wang, Y.; Su, H.; Xu, C.; Li, G.; Gell, L.; Lin, S.; Tang, Z.; Häkkinen, H.; Zheng, N., *J. Am. Chem. Soc.* **2015**, *137*, 4324-4327.
32. Zhang, R.; Hao, X.; Li, X.; Zhou, Z.; Sun, J.; Cao, R., *Cryst. Growth Des.* **2015**, *15*, 2505-2513.
33. Chakrahari, K. K.; Liao, J.-H.; Kahlal, S.; Liu, Y.-C.; Chiang, M.-H.; Saillard, J.-Y.; Liu, C. W., *Angew. Chem. Int. Ed.* **2016**, *55*, 14704-14708.
34. Wang, Y.; Su, H.; Ren, L.; Malola, S.; Lin, S.; Teo, B. K.; Häkkinen, H.; Zheng, N., *Angew. Chem. Int. Ed.* **2016**, *55*, 15152-15156.
35. Lei, Z.; Wan, X.-K.; Yuan, S.-F.; Wang, J.-Q.; Wang, Q.-M., *Dalton Trans.* **2017**, *46*, 3427-3434.
36. Wan, X.-K.; Cheng, X.-L.; Tang, Q.; Han, Y.-Z.; Hu, G.; Jiang, D.-e.; Wang, Q.-M., *J. Am. Chem. Soc.* **2017**, *139*, 9451-9454.
37. Jin, J.-L.; Xie, Y.-P.; Cui, H.; Duan, G.-X.; Lu, X.; Mak, T. C. W., *Inorg. Chem.* **2017**, *56*, 10412-10417.
38. Wan, X. K.; Guan, Z. J.; Wang, Q. M., *Angew. Chem. Int. Ed.* **2017**, *56*, 11494–11497.
39. Qu, M.; Li, H.; Xie, L.-H.; Yan, S.-T.; Li, J.-R.; Wang, J.-H.; Wei, C.-Y.; Wu, Y.-W.; Zhang, X.-M., *J. Am. Chem. Soc.* **2017**, *139*, 14346-12349.
40. Yuan, S.-F.; Li, P.; Tang, Q.; Wan, X.-K.; Nan, Z.-A.; Jiang, D.-e.; Wang, Q.-M., *Nanoscale* **2017**, *9*, 11405-11409.
41. Wang, Y.; Wan, X.-K.; Ren, L.; Su, H.; Li, G.; Malola, S.; Lin, S.; Tang, Z.; Häkkinen, H.; Teo, B. K.; Wang, Q.-M.; Zheng, N., *J. Am. Chem. Soc.* **2016**, *138*, 3278-3281.
42. Chui, S. S. Y.; Ng, M. F. Y.; Che, C.-M., *Chem. Eur. J.* **2005**, *11*, 1739-1749.
43. Shao, C.; Cheng, G.; Su, D.; Xu, J.; Wang, X.; Hu, Y., *Adv. Synth. Catal.* **2010**, *352*, 1587-1592.
44. Freitag, K.; Banh, H.; Gemel, C.; Seidel, R. W.; Kahlal, S.; Saillard, J.-Y.; Fischer, R. A., *Chem. Commun.* **2014**, *50*, 8681-8684.
45. Ganesamoorthy, C.; Weßing, J.; Kroll, C.; Seidel, R. W.; Gemel, C.; Fischer, R. A., *Angew. Chem. Int. Ed.* **2014**, *53*, 7943-7947.
46. Yang, H.; Lei, J.; Wu, B.; Wang, Y.; Zhou, M.; Xia, A.; Zheng, L.; Zheng, N., *Chem. Commun.* **2013**, *49*, 300-302.
47. Yang, H.; Wang, Y.; Zheng, N., *Nanoscale* **2013**, *5*, 2674-2677.
48. Kang, X.; Wang, S.; Song, Y.; Jin, S.; Sun, G.; Yu, H.; Zhu, M., *Angew. Chem. Int. Ed.* **2016**, *55*, 3611-3614.
49. van der Velden, J. W. A.; Bour, J. J.; Vollenbroek, F. A.; Beurskens, P. T.; Smits, J. M. M., *J. Chem. Soc., Chem. Commun.* **1979**, 1162-1163.
50. Demartin, F.; Manassero, M.; Naldini, L.; Ruggeri, R.; Sansoni, M., *J. Chem. Soc., Chem. Commun.* **1981**, 222-223.
51. Zeller, E.; Beruda, H.; Schmidbaur, H., *Inorg. Chem.* **1993**, *32*, 3203-3204.
52. Saillard, J.-Y.; Halet, J.-F., Structure and Bonding Patterns in Large Molecular Ligated Metal Clusters. In *The Chemical Bond I: 100 Years Old and Getting Stronger*, Mingos, D. M. P., Ed. Springer International Publishing: Cham, 2016; pp 157-179.
53. Tornøe, C. W.; Christensen, C.; Meldal, M., *J. Org. Chem.* **2002**, *67*, 3057-3064.
54. Rostovtsev, V. V.; Green, L. G.; Fokin, V. V.; Sharpless, K. B., *Angew. Chem. Int. Ed.* **2002**, *41*, 2596-2599.
55. Makarem, A.; Berg, R.; Rominger, F.; Straub, B. F., *Angew. Chem. Int. Ed.* **2015**, *54*, 7431-7435.
56. Jin, L.; Tolentino, D. R.; Melaimi, M.; Bertrand, G., *Sci. Adv.* **2015**, *1*, e1500304.
57. Meldal, M.; Tornøe, C. W., *Chem. Rev.* **2008**, *108*, 2952-3015.
58. Alonso, F.; Moglie, Y.; Radivoy, G., *Acc. Chem. Res.* **2015**, *48*, 2516-2528.
59. Lee, B.-H.; Wu, C.-C.; Fang, X.; Liu, C. W.; Zhu, J.-L., *Catal. Lett.* **2013**, *143*, 572-577.
60. Decan, M. R.; Impellizzeri, S.; Marin, M. L.; Scaiano, J. C., *Nat. Commun.* **2014**, *5*, 4612.
61. Lipshutz, B. H.; Taft, B. R., *Angew. Chem. Int. Ed.* **2006**, *45*, 8235-8238.
62. Sharghi, H.; Khalifeh, R.; Doroodmand, M. M., *Adv. Synth. Catal.* **2009**, *351*, 207-218.
63. Alonso, F.; Moglie, Y.; Radivoy, G.; Yus, M., *Adv. Synth. Catal.* **2010**, *352*, 3208-3214.
64. Lee, B. S.; Yi, M.; Chu, S. Y.; Lee, J. Y.; Kwon, H. R.; Lee, K. R.; Kang, D.; Kim, W. S.; Lim, H. B.; Lee, J.; Youn, H.-J.; Chi, D. Y.; Hur, N. H., *Chem. Commun.* **2010**, *46*, 3935-3937.
65. Alonso, F.; Moglie, Y.; Radivoy, G.; Yus, M., *Org. Biomol. Chem.* **2011**, *9*, 6385-6395.
66. Nador, F.; Volpe, M. a. A.; Alonso, F.; Feldhoff, A.; Kirschning, A.; Radivoy, G., *Appl. Catal., A* **2013**, *455*, 39–45.
67. Rance, G. A.; Solomonsz, W. A.; Khlobystov, A. N., *Chem. Commun.* **2013**, *49*, 1067-1069.

68. Sarmah, B.; Satpati, B.; Srivastava, R., *RSC Adv.* **2016**, *6*, 87066-87081.

69. Molteni, G.; Bianchi, C. L.; Marinoni, G.; Santo, N.; Ponti, A., *New J. Chem.* **2006**, *30*, 1137-1139.

70. Abdulkin, P.; Moglie, Y.; Knappett, B. R.; Jefferson, D. A.; Yus, M.; Alonso, F.; Wheatley, A. E. H., *Nanoscale* **2013**, *5*, 342-350.

71. Fu, F.; Martinez, A.; Wang, C.; Ciganda, R.; Yate, L.; Escobar, A.; Moya, S.; Fouquet, E.; Ruiz, J.; Astruc, D., *Chem. Commun.* **2017**, *53*, 5384-5387.

72. Gaur, S.; Miller, J. T.; Stellwagen, D.; Sanampudi, A.; Kumar, C. S. S. R.; Spivey, J. J., *Phys. Chem. Chem. Phys.* **2012**, *14*, 1627-1634.

73. Wu, Z.; Hu, G.; Jiang, D.-e.; Mullins, D. R.; Zhang, Q.-F.; Allard, L. F.; Wang, L.-S.; Overbury, S. H., *Nano Lett.* **2016**, *16*, 6560-6567.

TOC Graphic